Microstructure Organization in Para-aramid Fibers

Hawthorne Davis, James Singletary, Mohan Srinivasarao, Warren Knoff and M.K. Ramasubramanian

Textile Research Journal 2000; 70; 945
DOI: 10.1177/004051750007001102

Microstructure Organization in Para-aramid Fibers

HAWTHORNE DAVIS[1] AND JAMES SINGLETARY

College of Textiles, North Carolina State University, Raleigh, North Carolina 27695, U.S.A.

MOHAN SRINIVASARAO

Department of Textiles Engineering, Georgia Institute of Technology, Atlanta, Georgia 30332, U.S.A.

WARREN KNOFF

DuPont Advanced Fiber Systems, Richmond, Virginia 23261, U.S.A.

M. K. RAMASUBRAMANIAN

College of Engineering, North Carolina State University, Raleigh, North Carolina 27695, U.S.A.

ABSTRACT

The existence of "lateral birefringence," *i.e.*, the difference between the refractive index for light polarized parallel to the fiber radius and light polarized perpendicular to the radius in the cross-sectional plane, combined with the existence of electron diffraction contrast "bands" in longitudinal fiber sections has led to work appearing to indicate that para-aramid fibers, in particular poly(para-phenylene terephthalamide), have an almost crystallographically perfect orthotropic structure in which the hydrogen bonds are all parallel to fiber radii. Optical path difference profiles, calculated based on the proposed orthotropic structure, are in reasonable qualitative agreement with interference microscope data. Quantitatively, however, the orthotropic structure is only partially developed based on published values of the principle refractive indices. Furthermore, the degree to which this structure is developed varies with distance from the fiber axis in some fibers' types.

High strength poly(para-phenylene terephthalamide) (PPTA) fibers are commercially produced on a large scale by a spinning process in which a lyotropic solution of the polymer in sulfuric acid is extruded through a capillary, attenuated in an air gap, and quenched in an aqueous medium. The original description [1] of this fiber in the patent literature indicated it is truly different from other fibers. Whereas most fibers, when viewed along their axes, appear isotropic apart from occasional spherulitic structures (that is, every region approaching optically significant size in the usual fiber structure has a uniaxial indicatrix), PPTA fibers have a macroscopic structural organization something like a single spherulite growing radially from the fiber axis. This is a more complicated anisotropy than that in other fibers, and it results from the *b* crystallographic axis (or the hydrogen bonding direction) tending to be aligned parallel to the radial vectors. The literature has used various terms to describe this structure, and for clarity we will call it "radial orthotropy" (RO).

RO produces a "lateral birefringence," which has been measured on fiber sections and at least once previously on whole, nonsectioned fibers. The implicit assumption that this structure is highly, or even perfectly, developed has led to interpretation of various structural data, *e.g.*, the "pleated sheet structure," originally observed by the late R. G. Scott [5] and studied in detail by Dobb *et al.* [3] as almost crystallographic in origin. Following Dobb and Johnson, Warner [6] reported that the interference microscope fringe shift pattern characteristic of these fibers results not from a radial profile of orientation or crystallinity as in other fibers, but from this RO. Since Warner's measurements could not have damaged the fibers, these observations strengthened the case for a highly perfect structure. Warner, however, did not report an analysis showing how the proposed structure would be expected to produce his distinctive interference microscope results. Yabuki *et al.* [8] also observed this radial structure with interference microscopy, albeit of

[1] Author to whom correspondence should be addressed.

  0040-5175/$2.00

fiber sections, and proposed an apparently perfect RO structure for the near surface region (sheath) with a randomized, or rather locally uniaxial, core.

Current literature on this subject does not quantify in a satisfying manner the extent of RO responsible for these observations, justify the acceptance of a perfect pleated sheet structure, or attempt to identify differences in these features between fibers, *e.g.*, fibers produced by different processes or different manufacturers. In this paper, we attempt to describe and quantify this structure by measuring the shapes of interference fringes for several PPTA fibers and comparing them with computed profiles based on the RO model.

Theory

An interference microscope measures the optical path difference between two light rays that follow different paths to the same point in an image. For studying fibers, the system is arranged such that one of these rays travels through an immersion medium of known refractive index n_0. The other ray passes through the fiber. The ray inside the fiber generally follows a curved path, which can be difficult to determine as reported by Wu *et al.* [7]. Since a refractive index usually changes slowly inside a fiber, the ray path can be approximated by a straight line parallel to the microscope axis. We will make this assumption for a first analysis of this problem. Under this assumption, it is straightforward to calculate an expected interference fringe shift profile for the assumed orthotropic structure of aramid fibers.

According to the orthotropic model structure, the indicatrix at any point is represented by an ellipsoid, which has principal refractive indices $n_1 = 1.73$, $n_2 = 1.51$, and $n_3 = 2.05$, as estimated by Yabuki *et al.* [8] using the method of Denbigh [2]. For light polarized perpendicular to the fiber axis, the indicatrix can be represented by the ellipse,

$$\frac{\xi^2}{n_1^2} + \frac{\varsigma^2}{n_2^2} = 1 \quad . \tag{1}$$

In the orthotropic model of aramid fiber structure, the minor axis of the indicatrix (n_2) is always perpendicular to the fiber radius. Thus, a light ray passing through the fiber along a line $x = x_0$ encounters a continuously changing refractive index $n(y, x_0)$, which is conveniently calculated if refraction is ignored. In Figure 1, the light ray is assumed to follow the path $x = x_0$. This light ray is retarded relative to a ray that passes through the immersion liquid by an amount $OPD(x_0)$, where

$$OPD(x_0) = \int_a^b n(y)dy - n_0 \int_a^b dy \quad . \tag{2}$$

The integral is taken along the path of the light ray, which is assumed to be $x = x_0$. Along this path, the angle θ between the n_2 axis of the indicatrix and the x axis is given by

$$\tan \theta = \frac{x_0}{y} \quad . \tag{3}$$

This leads to a local value of the refractive index seen by the traversing light ray, which varies with distance y from the x axis in Figure 1:

$$n(y, x_0) = \frac{n_1 n_2}{\sqrt{n_1^2 \sin^2 \theta + n_2^2 \cos^2 \theta}} = \frac{n_1 n_2 \sqrt{y^2 + x_0^2}}{\sqrt{n_1^2 x_0^2 + n_2^2 y^2}} \quad . \tag{4}$$

The optical path difference for each point x_0, *i.e.*, the fringe shift profile, was evaluated numerically using the trapezoidal rule method given by Press *et al.* [4]. Note that this analysis ignored internal refraction for simplicity. The experiments we report have been designed to minimize error from external refraction.

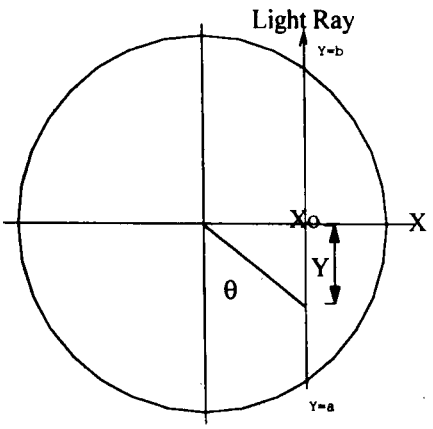

FIGURE 1. Schematic showing assumed straight line ray path through fiber and giving nomenclature.

Experimental Methods

Single fiber specimens were fastened to microscope slides and immersed in a liquid that matched the surface refractive index. The electric vector **E** of the Hg green light used was set perpendicular to the axis of the fiber. Thus, at the edge of the fiber image, **E** was parallel to the fiber radius vector, and therefore to the hydrogen bond direction, which has refractive index n_1. For light that passed exactly along the diameter of the fiber, **E** was

everywhere perpendicular to the hydrogen bond direction and should see the refractive index n_2.

The immersion liquid refractive index n_0 was matched to the refractive index at the fiber surface within ± 0.002, so n_1 was determined directly. This index match was judged based on the absence of an abrupt fringe shift at the fiber/liquid interface. As is well known, if the refractive index is matched perfectly, the edge of the fiber is invisible, and the position of the edge of the fiber is indeterminate. This means the fiber diameter is difficult to determine accurately. The fiber diameter for the Kevlar items was estimated from the dpf (a measure of linear density used in textiles: the mass of a 9000 m length of a single fiber) and density.

We measured interference fringe patterns by digitizing the analog signal from a monochrome CCD TV camera with a Targaplus video digitizer. Computer software facilitated aligning the fiber precisely with the scan direction, and orienting the interference fringes outside the fiber perpendicular to this direction. Scan lines consisting of 512 data points were taken from about eight lines outside the fiber on one edge of the fiber image to eight lines outside the other edge. Slight sloping of the base line was removed by least squares fitting data points outside the fiber and subtracting the effect of any slope. Ten to twelve interference fringes were visible in the microscope field. These were digitized, and the fringe shift from the baseline was extracted as a phase from an FFT of the sinusoidal intensity pattern. This method has been tested extensively and found to give the same result as the slower, nonlinear least squares fit to the sinusoidal intensity function described in Wu *et al.* [7].

The refractive indices n_0 of the Cargile immersion liquids were converted from 589 to 546 nm using Cargile's data. Error attributable to this approach is an insignificant factor in this work.

MATERIALS

The materials examined are described in Table I. These samples represent a range of products available today. We chose them to test whether the orthotropic structure observed depends on heat treatment or factors related to fiber diameter and manufacturer-specific process details not available to us.

TABLE I. Description of samples used in these experiments.

Sample code	Sample ID
A	1.5 dpf (10 μm diameter) Kevlar[a] 29
B	6.0 dpf (20 μm diameter) experimental fiber like Kevlar 29
D	1.5 dpf Twaron[b] fiber with moderate heat treatment
E	1.5 dpf Twaron fiber with severe heat treatment

[a] DuPont trademark for its para-aramid fibers. [b] AKZO trademark for its para-aramid fibers.

Results

Figure 2 shows a typical interference fringe shift pattern from sample B. The general shape of these fringe patterns is similar for all the samples. In melt-spun fibers, where the fringe shape is determined by orientation and crystallinity variation within the fiber, the fringe shape is different from Figure 2. In melt-spun fibers, the maximum slope of the fringes is at the fiber/liquid interface, and there is always a substantial region of nearly zero slope near the center of the fiber image. In Figure 2 and the remaining figures in this paper, absolute values of the fringe shifts are plotted. In every case, a positive fringe shift indicates an algebraically smaller optical path. Determining n_1 and n_2 from such interference microscopy data is straightforward. We estimated the radii of the Twaron fibers from the images.

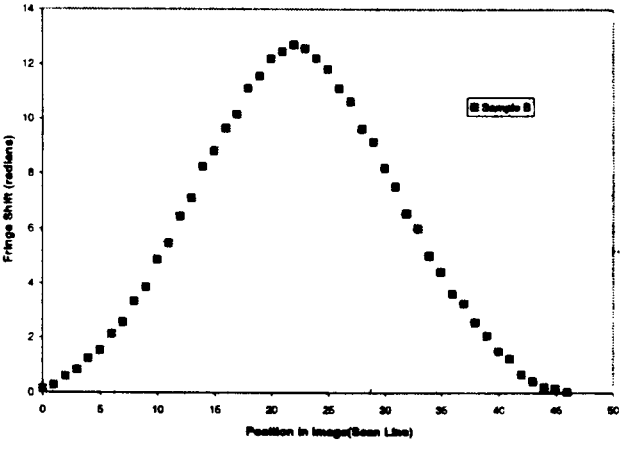

FIGURE 2. Interference fringe profile for sample B.

Table II compares the observed refractive indices with the calculated unit cell values obtained from reference 8. It is apparent in this table that the lateral birefringence measured in these fibers is ⅕–⅓ of that expected based on Yabuki *et al.* [8]. It is possible that the radii of the Twaron fibers shown are low by a few tenths of 1 μm. Should the fiber radii be larger than the estimates shown, the actual values for radial birefringence would also be smaller by about 0.004.

Figures 3 and 4 compare fringe shapes, calculated using the data in Table II, with observed data. Because the model is radially symmetrical, the data were averaged into radial "half fringe patterns" by the following

TABLE II. Measured principle refractive indices.

Item	n_1	n_2	Radial Δn	Radius, μm
Perfect RO	1.73	1.51	0.22	–
A	1.6556	1.6213	0.034	6.1
B	1.6556	1.6110	0.045	12.2
D	1.6638	1.6034	0.060	5.5
E	1.6804	1.6134	0.067	5.0

method: The center of each fiber was located by finding the point, to within ⅛ of a pixel, at which the sum of squares of differences between the right-hand and left-hand fringe displacements was minimum. A cubic spline was used for interpolation, and results shown represent averages of the left- and right-hand sides of the image. Since aramid fibers have practically perfect radial symmetry, this operation hardly changed the data.

Figure 3 shows the two Kevlar fibers. The sample A fringe profile agrees perfectly with the RO calculation. The radial birefringence is, however, only 15% of that expected based on the unit cell calculations [8]. Sample B data fit the orthotropic model well near the fiber surface, but deviate toward the low refractive index direction near the fiber core.

Figure 4 compares results for the two Twaron fibers, D and E. Both these fibers had been heat treated and were more crystalline than the Kevlar fibers. The radial birefringence of D and E was about 30% of the value expected from the perfect orthotropic model, but could be slightly lower as we explained earlier. These fringe shapes deviated from the RO prediction much like, but perhaps more strongly than, those for sample B.

Discussion

With the exception of Warner's work [6], previous measures of lateral birefringence in aramid fibers [1, 8] were made on fiber sections, which could have been damaged. Warner stated, but offered no proof, that the

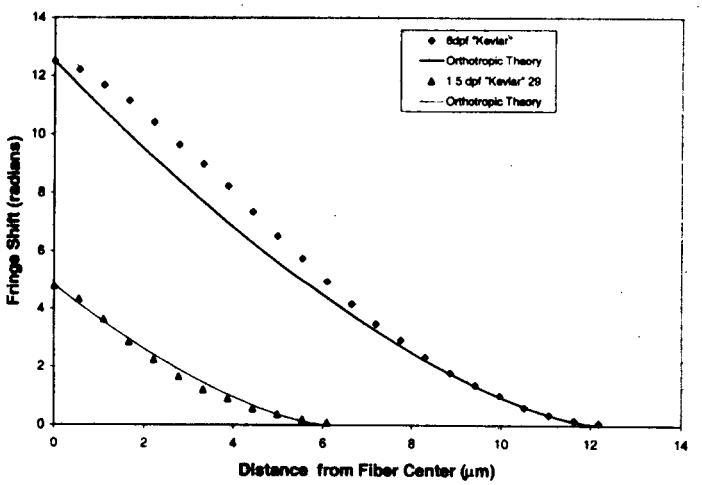

FIGURE 3. Interference fringe profile for Kevlar fibers.

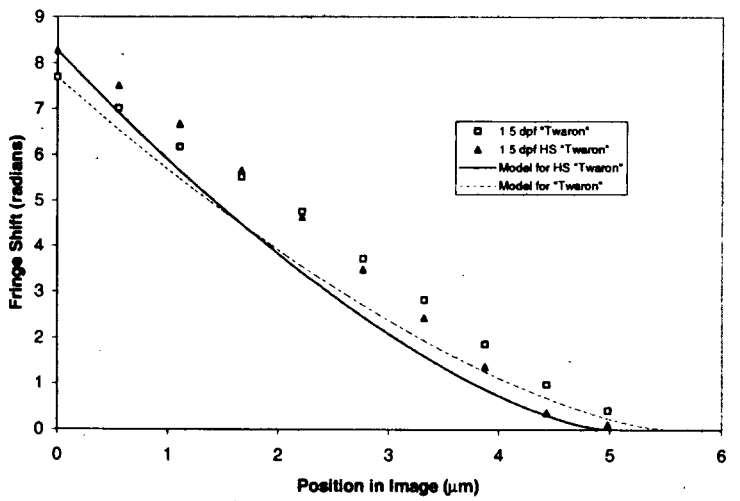

FIGURE 4. Fringe profiles for 1.5 dpf Twaron fibers.

observed interference fringe profiles, which are comparable to those reported here, were a result of RO and not of surface-to-core variation in axial orientation or crystallinity. The work we present here shows that the interference fringe shapes observed for several kinds of PPTA fibers reasonably approximate, in the absence of complications from internal refraction, the expectation from RO. Further, these fringe profiles are unlike those observed in melt spun fibers where there is no detectable RO.

The principle radial refractive indices and radial birefringences observed differ considerably from those expected for fibers with perfect RO. Yabuki *et al.* [8] noted a similar discrepancy by a different and more invasive procedure, and proposed that a reasonable model for the structure would be a perfectly ordered skin region over a core, which has local radial isotropy like conventional melt spun fibers.

GENERALIZATION OF THE YABUKI MODEL

Based on our work, the hypothesis of a truly RO structure anywhere in these fibers is not tenable. The data for sample A fit the RO model perfectly. The measured radial birefringence is, however, far too low. A model based on a partly RO structure, which is independent of distance from the fiber axis, would fit the observations for this fiber. In this model, a primary crystal axis, *e.g.*, the hydrogen bond direction, is symmetrically distributed about the radial direction. This could be described, *e.g.*, by a distribution function for the hydrogen bond direction $P(\theta)$, where the angle θ is measured from the local radial vector, of the form

$$P(\theta)d\theta = Ne^{-\alpha\theta^2}d\theta \quad , \qquad (5)$$

where N is a normalizing factor and $1/\alpha$ represents the breadth of the distribution. In sample A the (assumed positive) parameter α is independent of radial position. In the remaining samples, α would need to increase with distance from the center of the fiber to account for the observations. This concept is a reasonable generalization of the model proposed by Yabuki *et al.* [8]. The analysis developed in this work could be used to estimate a radial-position dependence of α. Before going to this trouble, we think the theory should be corrected for internal refraction, and it is not clear at this point whether the work is justified.

CORRELATION OF RADIAL BIREFRINGENCE WITH DEVIATION FROM ORTHOTROPIC STRUCTURE

In Figures 3 and 4, the extent to which fringe shape deviates from RO expectation increases as the estimated radial birefringence increases. This correlation would survive reasonable allowance for uncertainty in fiber diameter. Our qualitative observation is consistent in other filaments from the same items. Radial birefringence also appears to increase with overall refractive index, which apparently is related to heat treatment and consequently density. Insufficient work has been done to determine the cause of these correlations, which we present at this point as trends apparent in the data.

So far we have made no attempt to determine whether the samples we studied are representative of the product. Having studied sufficient fibers, we are confident that the general results reported here are representative of the samples we examined, and detailed work on the products will be left to the fiber producers.

IMPERFECT ORTHOTROPIC STRUCTURES

Earlier literature has not specifically claimed "perfect" RO for PPTA fibers, but it has stated that the hydrogen bonds are radially aligned, and has not defined this further. Perfect radial orthotropy would not be favored by strain energy considerations, and would result in an uncomfortable singularity at the fiber core. A similar problem occurs in mesophase pitch-based carbon fibers. Here, the literature seems to favor a model where {0001} zig-zags about the radial direction. It is not clear how literally this model should be taken or how crystallographic and correlated the zag angles might be. This model could also describe the PPTA observations if the zag angle depended on radial position.

FUTURE WORK

We did not correct the predicted fringe shapes for internal refraction because the analysis to do this has not been developed yet. We are now evaluating whether such a refraction-corrected analysis, *e.g.* along the lines of work by Wu *et al.* [7], is justified. The precision of the measurement system now available, combined with the high quality and uniformity of commercial aramid fibers, would probably permit improved understanding of the disorder responsible for the observations we have reported here.

Conclusions

Aramid fibers have a generally imperfect RO, in which the hydrogen bond direction is symmetrically distributed about the fiber radius vector. To a first approximation, the RO structure might be considered 20% formed. In some fibers, the perfection of the RO structure increases with distance from the center of the fiber.

ACKNOWLEDGMENTS

We acknowledge the DuPont Company, who provided Kevlar fibers and funded a graduate student on a project related to this work. We further acknowledge AKZO for providing Twaron fibers used in this study. Dr. Aparna Chidambaram, who performed the interference microscope experiments but was otherwise not connected with this work, is also gratefully acknowledged.

Literature Cited

1. Blades, H., High Strength Polyamide Fibers and Films, U.S. patent 3 869 430, 1974.
2. Dengigh, K. G., The Polarisibilities of Bonds, *Trans. Faraday Soc.* **36,** 936 (1940).
3. Dobb, M. G., Johnson, D., and Saville, B. P., Supramolecular Structure of a High-modulus Polyaromatic Fiber (Kevlar49), *J. Polym. Sci. Polym. Phys.* **15,** 2201 (1977).
4. Press, W. H., Flannery, B. P., Teukolsky, S. A., and Vetterling, W. T., "Numerical Recipes," Cambridge University Press, U.K., 1986.
5. Scott, Robert G., Personal communication, 1969.
6. Warner, S., On the Radial Structure of Kevlar, *Macromolecules* **16,** 1546 (1983).
7. Wu, Z., Davis, H. A., and Batra, S. K., Correct Ray-tracing Analysis for Interference Microscopy of Fibres, *Proc. R. Soc. Lond. A* **450,** 23–36 (1995).
8. Yabuki, K., Ito, H., and Ora, T., Consideration of the Relation between Fine Structure and Mechanical Properties of Poly(*p*-phenylene Terephthalamide) Fibers, *Sen-i Gakkaishi* **32,** T-56 (1976).

Manuscript received July 20, 1999; accepted October 13, 1999.

Woven Fabric Quality Evaluation Using Image Analysis

AKIO SAKAGUCHI, HYUNGSUP KIM, YO-ICHI MATSUMOTO, AND KOICHIRO TORIUMI

Department of Textile System Engineering, Shinshu University, Ueda, Nagano, Japan

ABSTRACT

As a factor important to fabric quality, reed marks are studied by theoretical and experimental methods. In order to analyze their appearance, the power spectrum of a fabric's image is simulated in terms of that fabric's geometry. These power spectra offer peaks of wavelength coincident with the reed spacing. Further, they are used as an indicator to explain reed marks in terms of packed warps. At this same wavelength in experimental power spectra, there is also a peak that exhibits dependence on fabric quality. This peak adequately describes the appearance of the reed marks and thus can be used as a quality indicator for a woven fabric.

Recently, advanced computer technology has contributed to various fields of the textile industry, such as quality control, machine automation, and high-speed machine operation. However, evaluating a fabric's surface still depends on the human eye and thus suffers the drawbacks of reliability due to human fatigue, speed, and overall accuracy. To avoid these disadvantages, researchers have tried to develop methods for fabric inspection that substitute for humans [1–9]. Recently, Zhang *et al.* [9] researched the detection of slubs and knots on woven fabrics, and at almost the same time, our research group also developed a method to detect oblique lines on woven fabrics using angular Fourier transformation [4]. Although those works opened a new era of image analysis for fabric inspection, they did not provide theoretical approaches, nor did they attempt any interpretations in terms of processing conditions. Our work reported here provides both theoretical insight and process interpretation.

Reed marks exhibit periodicity that depends on such manufacturing conditions as warp and reed spacing. Based on that periodicity and the fabric's geometry, the power spectrum of the fabric's image is simulated in an attempt to explain the appearance of reed marks on the